ACS Biomaterials SCIENCE & ENGINEERING

pubs.acs.org/journal/abseba

Article

Cobalt and Chromium Ions Impair Macrophage Response to *Staphylococcus aureus* Infection

Lea A. Tölken, Georgi I. Wassilew, Daniel Grolimund, Timm Weitkamp, Bernhard Hesse, Anastasia Rakow, Nikolai Siemens,*,▽ and Janosch Schoon*,▽

Cite This: *ACS Biomater. Sci. Eng.* 2024, 10, 563−574

Read Online

ACCESS | Metrics & More | Article Recommendations | Supporting Information

ABSTRACT: Cobalt−chromium−molybdenum (CoCrMo) alloys are routinely used in arthroplasty. CoCrMo wear particles and ions derived from arthroplasty implants lead to macrophage-driven adverse local tissue reactions, which have been linked to an increased risk of periprosthetic joint infection after revision arthroplasty. While metal-induced cytotoxicity is well characterized in human macrophages, direct effects on their functionality have remained elusive. Synchrotron radiation X-ray microtomography and X-ray fluorescence mapping indicated that peri-implant tissues harvested during aseptic revision of different arthroplasty implants are exposed to Co and Cr in situ. Confocal laser scanning microscopy revealed that macrophage influx is predominant in patient tissue. While in vitro exposure to Cr^{3+} had only minor effects on monocytes/macrophage phenotype, pathologic concentrations of Co^{2+} significantly impaired both, monocyte/macrophage phenotype and functionality. High concentrations of Co^{2+} led to a shift in macrophage subsets and loss of surface markers, including CD14 and CD16. Both Co^{2+} and Cr^{3+} impaired macrophage responses to *Staphylococcus aureus* infection, and particularly, Co^{2+}-exposed macrophages showed decreased phagocytic activity. These findings demonstrate the immunosuppressive effects of locally elevated metal ions on the innate immune response and support further investigations, including studies exploring whether Co^{2+} and Cr^{3+} or CoCrMo alloys per se expose the patients to a higher risk of infections post-revision arthroplasty.

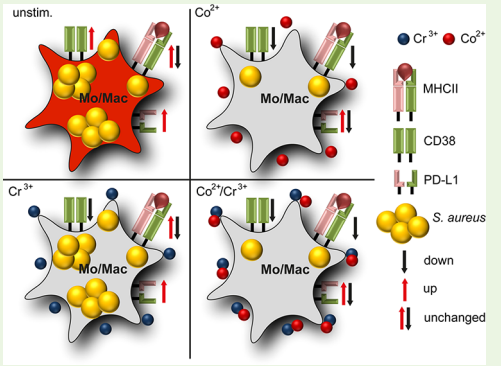

KEYWORDS: *macrophages, Staphylococcus aureus, arthroplasty, cobalt, chromium, periprosthetic joint infection*

1. INTRODUCTION

Arthroplasty is a successful surgical procedure for the treatment of patients suffering from chronic pain due to degenerative joint disease. Complications that usually occur in the late postoperative course due to tissue inflammation caused by material degradation and release or infections lead to revisions of implants. Cobalt−chromium-molybdenum (CoCrMo) metal alloys are metallic biomaterials widely used in arthroplasty. Multiple studies have indicated the adverse effects of wear particles and metal ions released from CoCrMo alloys. These adverse local tissue reactions (ALTRs), such as tissue necrosis and pseudotumor formation, are characterized by lymphocyte and macrophage infiltration.[1] Two specific types of necrosis occur in ALTRs, namely, (i) necrosis predominantly through death of macrophages and (ii) tissue necrosis characterized by cell death of stromal elements.[2] In vitro data indicate that macrophage necrosis and not apoptosis is the predominant type of cell death following exposure to high concentrations of Co^{2+}.[3] Widely accepted mechanisms posit that phagocytosis of arthroprosthetic metal particles activates the NLRP3 inflammasome and that the cellular damage caused by metal ions results in the release of proinflammatory cytokines, subsequently giving rise to the inflammatory responses observed in ALTRs.[4−6] The proinflammatory environment has been held responsible for the differentiation of macrophages to bone-resorbing osteoclasts and their activation, hence for the onset of periprosthetic osteolysis.[7] In clinical context, exposure to Co^{2+} and Cr^{3+} has been associated with early implant revision and increased rates of secondary revision, due to aseptic implant loosening and/or periprosthetic joint infections (PJI).[8−13] Factors such as metal-induced cytotoxicity as well as ALTRs are believed to create an environment favorable to bacterial infections.[14,15]

Previous studies have shown that peri-implant tissues, including bone marrow, are exposed to Co- and Cr-containing particles[2,16−18] and that these metals are present in the particulate as well as in the dissociated state.[19] The comparison between in vitro corrosion and tribocorrosion showed that the dissolution of Co occurred primarily in tribocorrosive

Received: July 27, 2023
Revised: December 4, 2023
Accepted: December 6, 2023
Published: December 18, 2023

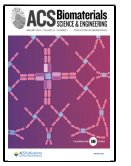

https://doi.org/10.1021/acsbiomaterials.3c01031
ACS Biomater. Sci. Eng. 2024, 10, 563−574

conditions, suggesting that the mechanism responsible for particle release affects their Co content.[20] Ex vivo analyses of the elemental composition of CoCrMo particles in periprosthetic bone marrow have revealed that Co content depends on their size.[21] The comparison of elemental ratios of CoCrMo-derived particles with the composition of the implanted bulk alloy showed that particle degradation results in the release of Co ions,[21] reaching local pathologic concentrations exceeding 10 μg/mL.[19] Besides CoCr alloy particles, trivalent Cr salts and oxides have been shown to be the predominant state of Cr in periprosthetic tissue collected during revisions of metal-on-metal hip implants.[18] Notably, Co has only been found colocalized with Cr in the elemental states, indicating that dissociated Co is released during the wear process or due to dealloying by passive or cell-mediated degradation processes.[17,18,21] Consequently, dissociated Co and Cr can cross cellular barriers leading to systemic exposure.[22−24]

Besides ALTRs, PJIs are devastating complications of arthroplasty, requiring revision surgery with partial or total exchange or explantation of the implant, debridement of necrotic and infected tissues, and effective antimicrobial treatment.[25−28] The incidence of PJIs is constantly increasing during the last decades. However, certain referral centers, particularly in Scandinavia, are reporting that the incidence appears to have leveled out after 2010.[14,29,30] *Staphylococcus aureus* is one of the major causes of bone and joint infections[31,32] including PJIs.[33−35] Being held responsible for up to 28% of PJIs, makes it one of the most prevalent pathogens in revision arthroplasty.[36−38]

As part of the innate immune axis, macrophages are of crucial importance in initiating an immediate response to highly inflammatory conditions, particularly infections. Tissue-resident macrophages are the first responders. They are involved in tissue homeostasis, clearance of cellular debris as well as pathogens, and metallic particles, among others.[39,40] As a result of inflammation, the limited number of resident macrophages is depleted, and circulating monocytes influx into the tissue and differentiate into macrophages.[41] High influx of macrophages is commonly detected in peri-implant tissue, especially in ALTRs, and macrophages often colocalize with metal particles.[2] Metal particles as well as ions have been shown to impact macrophage viability,[42] migration,[43] and activation.[1] However, the pathogen-macrophage interplay following metal exposure remained unknown.

Thus, the aims of this study were to evaluate whether exposure to Co and Cr and subsequent macrophage influx is evident at the time of aseptic arthroplasty implant revision and to analyze the impact of Co and Cr ions on human primary monocytes/macrophages, including markers associated with infections and the ability of these cells to respond to subsequent *S. aureus* infection. We show that macrophages change their phenotype after Co^{2+} exposure. More strikingly, Co^{2+} affects the expression of various surface markers and impairs overall macrophage response to *S. aureus* infection. In contrast, Cr^{3+} does not significantly affect monocyte/macrophage phenotype but the response to infection.

2. MATERIALS AND METHODS

2.1. Patient Recruitment and Sampling. The independent ethics committee (IEC) of the University Medicine Greifswald approved the study (BB 178/20 and BB 014/14) in accordance with the World Medical Association Declaration of Helsinki. All patients gave written informed consent to participate in this study. All experiments were carried out in accordance with the approved guidelines. Peri-implant soft tissue samples were collected during aseptic arthroplasty implant revisions. Buffy coats obtained from healthy blood donors were anonymously provided by the Blood Bank of the University Medicine Greifswald.

2.2. Synchrotron Radiation X-ray Computed Tomography. Peri-implant soft tissue samples were fixed in phosphate-buffered saline (PBS, BIO SELL) containing 4% v/v formaldehyde (Carl Roth). Following overnight fixation, the specimens were placed in 2 mL screw-top tubes filled with PBS containing 100 U/mL penicillin and 1 μg/mL streptomycin (both Gibco). The specimens were scanned using Synchrotron radiation microcomputed tomography (SR-μCT) at the Anatomix beamline at the Synchrotron SOLEIL; the beamline and its instrumentation are described elsewhere.[44,45] In brief, the voxel size was 3.07 μm^3, and the central energy of the filtered white X-ray beam was around 40 keV. Each scan involved a slight offset of the rotation axis in relation to the detector field of view, aiming to enlarge the diameter of the reconstructed volume. For each scan, between 3000 and 4000 projections were acquired, each with an exposure time of 50 ms per projection. For the reconstruction of tomographic data, the standard pipeline implemented at the beamline was used; it is based on the PyHST2 framework. A Paganin phase-retrieval filter with a kernel length ("Paganin length" in PyHST2) of 138 μm was applied to facilitate data analysis.

Further data analysis and visualization of the tomographic reconstructions was performed using the AVIZO software (Thermo Fisher Scientific). For the segmentation of metallic particles, the 3D images were thresholded, selecting a value above the gray values corresponding to mineralized tissue. Subsequently, only particles larger than 4 voxels were considered as metal particles.

2.3. Synchrotron Radiation X-ray Fluorescence Mapping. Parts of the fixed specimens (see Section 4) were dehydrated for 24 h in each step by an ascending ethanol gradient (70, 80, 96, and 100%). After completion of dehydration by incubation with xylene (Th. Geyer) for 3 h, the specimens were embedded in paraffin, and 10 μm sections were prepared. The sections were placed between two pieces of a 4 μm thin ultralene foil (Spex SamplePrep) and mounted on custom-made sample holders. Synchrotron radiation micro X-ray fluorescence (SR-μXRF) mapping was performed at the microXAS beamline of the Swiss Light Source (Paul Scherrer Institute). Monochromatic excitation radiation of 9.8 keV (above the Zn K-edge) was selected using a double-crystal monochromator equipped with Si(111) crystals. The primary beam was focused by two orthogonal reflective mirrors (Kirkpatrick-Baez geometry) down to a spot size of 1 μm × 2 μm ($h \times v$). XRF spectra were collected using silicon drift detector systems. Chemical images were recorded in "on-the-fly" mode, with a pixel size of 20 μm × 20 μm to obtain overviews for further selection of regions of interest to be scanned with a pixel size of 2 μm × 2 μm. XRF spectra obtained for each individual pixel were deconvoluted using the software PyMCA.[46]

2.4. Histology, Immunostaining, and Laser Scanning Microscopy. The paraffin-embedded tissue samples used for sectioning and subsequent SR-XRF analyses were additionally sectioned for histology (5 μm) and immunostaining (10 μm). The sections were mounted on glass slides, dried overnight at 60 °C, and dewaxed with xylene prior to rehydration by ethanol gradient (100, 96, 80, 70%) and water. The section adjacent to the section used for immunostaining was stained with hematoxylin and eosin (both Carl Roth) by the "progressive method".[47] For immunostaining, antigen retrieval was performed by heating the slides in a microwave submersed in citrate buffer (pH 6.0, Sigma-Aldrich) until boiling followed by 10 min at a sub-boiling temperature (95−98 °C). Tissue sections were permeabilized with 1% saponin in PBS for 30 min at room temperature. Sections were blocked using 2.5% fetal calf serum (Gibco) and 2.5% normal goat serum (Abcam) in PBS for 30 min at room temperature. Sections were stained overnight at 4 °C by using titrated amounts of fluorophore-labeled antibodies. Sections were washed with PBS containing 1% saponin in between each staining step. The following antibodies were used for immunofluorescence analysis (clone, fluorophore; all BioLegend): CD68 (Y1/82A,

https://doi.org/10.1021/acsbiomaterials.3c01031
ACS Biomater. Sci. Eng. 2024, 10, 563−574

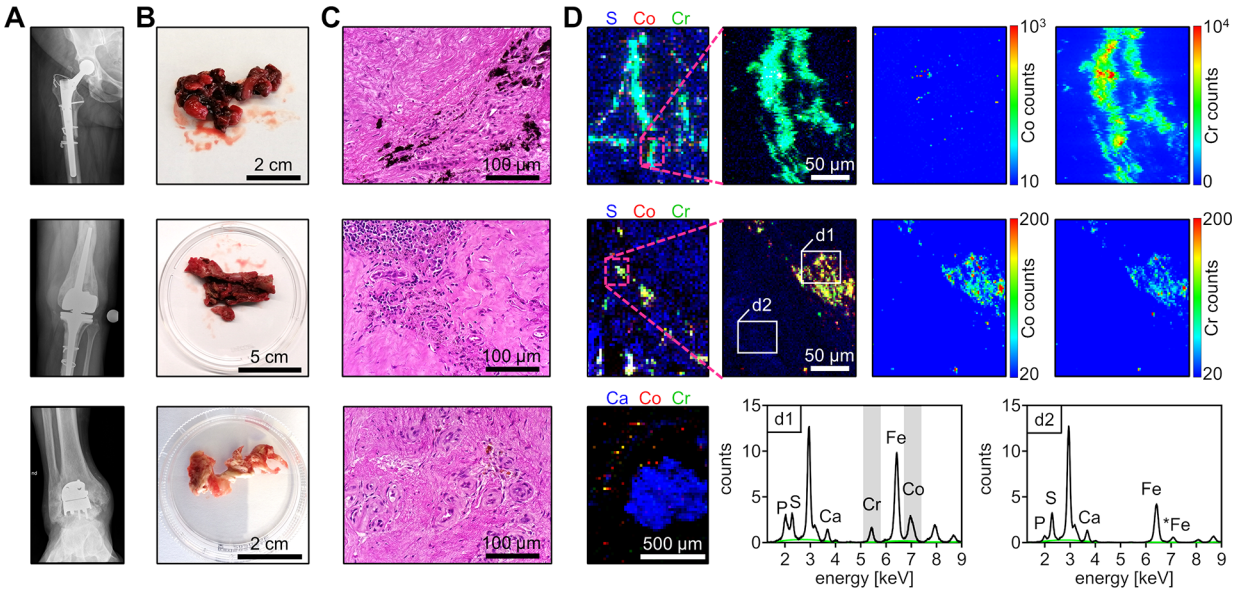

Figure 1. Histological evaluation and multielement detection of peri-implant tissue collected from three patients undergoing arthroplasty implant revision. The respective samples, tissue stains, and XRF maps are arranged horizontally. (A) From top to bottom: anteroposterior radiographs taken before revision of hip, knee, and ankle arthroplasty implants. (B) Peri-implant soft tissue samples. (C) Hematoxylin and eosin staining of tissue sections. (D) RGB imaging, heatmaps of the Co and Cr signals, and spectra of XRF maps of tissue sections at 20 μm steps (left) and 2 μm steps (right). RGB images (2 μm steps) depict the same region depicted by heatmaps.

AlexaFlour647), CD45/2D1, AlexaFlour700), CD14 (HCD14, AlexaFlour594) and HLA-DR (L243, AlexaFlour488). The staining was visualized using a Leica DMi8 CS Premium confocal laser scanning microscope (Leica).

2.5. Isolation of Human Monocytes and In Vitro Metal Exposure. Human monocytes were isolated from buffy coats using CD14 S-pluriBead antihuman beads (PluriSelect) according to the manufacturer's instructions. Cobalt(II) chloride hexahydrate and chromium(III) chloride hexahydrate (both Sigma-Aldrich) were dissolved in human AB serum (PAN-Biotech) at a stock concentration of 10 mg × mL^{-1} Co^{2+} or 10 mg/mL $Cr^{3+}$and 10 mg × mL^{-1} Co^{2+} plus 10 mg × mL^{-1} Cr^{3+} and incubated overnight at 37 °C. Preincubation was performed to emulate the in vivo formation of ion complexes of biomacromolecules. Isolated monocytes were exposed to metal salt solutions for 48 h at 37 °C and 5% CO_2 (final concentrations: 1 μg × mL^{-1} and 10 μg × mL^{-1} or of each in combination). Pure human AB serum served as control.

2.6. Bacterial Strain. *S. aureus* strain 6005[48] was grown overnight at 37 °C in casein hydrolysate and yeast extract medium with agitation.[49] To mimic initial low-grade infections, a multiplicity of infection (MOI) of 1 was used.

2.7. Infection of Monocytes/Macrophages. Stimulated monocytes were infected with *S. aureus* 6005 at an MOI of 1 for 1 h. Extracellular bacteria were killed by the addition of antibiotics (400 μg × mL^{-1} gentamicin/2 μg × mL^{-1} lysostaphin, both Sigma-Aldrich). For flow cytometry, infected monocytes were incubated for an additional 23 h at 37 °C and 5% CO_2. For the assessment of intracellular bacterial counts, monocytes were infected as described above. One hour after the addition of antibiotics, cells were washed, lysed, and intracellular bacteria were plated on blood agar plates (Oxoid).

2.8. Flow Cytometry. Dead cells were stained using the Zombie Aqua Fixable Viability Kit (BioLegend) according to the manufacturer's instructions. Human TruStain FcX (BioLegend) was used according to the manufacturer's instructions to block unspecific binding of immunoglobulins. Extracellular markers were stained by incubating the cells with titrated amounts of monoclonal antibodies at 4 °C for 30 min. Cells were fixed and permeabilized using the Cyto-Fast Fix/Perm Buffer Set (BioLegend). Intracellular markers were stained by using titrated amounts of monoclonal antibodies at 4 °C for 30 min. Cells were washed between each staining step. Antibodies and clones directed against the following markers were used (clone and fluorophore; all BioLegend): CD14 (63D3, BV750 or HCD14, PE/Cy7), CD16 (B73.1, PE/Dazzle594), HLA-DR (LN3, FITC), CD38 (HB-7, PerCP), CD86 (BU63, PE/Cy7), PD-L1 (29E.2A3, APC), and CD68 (Y1/82A, BV421). The gating strategy is shown in the Supporting Information (Figure S1). Data were acquired using a FACSAriaIII flow cytometer and FACS DIVA 8.0 Software (both BD Biosciences) and analyzed using FCS Express 7 Software (De Novo Software).

2.9. Quantitative Reverse Transcription PCR Analysis. Total RNA was isolated using the RiboPure RNA purification Kit (Ambion) according to the manufacturer's guidelines. cDNA synthesis was performed using the Superscript first-strand synthesis system for RT-PCR (Invitrogen). The real-time PCR amplification was performed with an iTaq Universal SYBR Green Supermix kit (Biorad) using a StepOnePlus sequence detection system (Applied Biosystems). The levels of β-actin transcription (h_beta-actin_for: 5′-CTCTTCCAGCCTTCCTTCCT-3′, h_beta-actin_rev: 5′-AG-CACTGTGTTGGCGTACAG-3′ (both Eurofins)) were used for normalization. The following commercially available primers were used (Name (cat. no.); all Qiagen): Hs_HLA_DRA_1_SG (QT00089383), Hs_CD68_1_SG (QT00037184), Hs_PPARG_1_SG (QT00029841), Hs_STAT1_1_SG (QT00074123), and Hs_IRF5_1_SG (QT00092736).

2.10. Statistics. The statistical significance of differences was determined using the Kruskal–Wallis test with Dunn's multiple comparison posttest. Data plotting and exploratory analyses were performed using GraphPad Prism version 8. A *p*-value below 0.05 was considered to be statistically significant. The analyses included all samples and data, and individual values were presented for all data points. The PyMCA software was used to perform RGB imaging, heatmap imaging, and peak spectra analyses of the XRF data.[46]

3. RESULTS

3.1. Local Metal Exposure and Macrophage Influx in Patient Tissue. To evaluate whether patients are locally exposed to Co- and Cr-containing degradation products, peri-implant tissue samples were collected during aseptic revision surgery of hip, knee, and ankle arthroplasty implants (n = 3) (Figure 1A,B).

https://doi.org/10.1021/acsbiomaterials.3c01031
ACS Biomater. Sci. Eng. 2024, 10, 563−574

Histological analysis of the tissue samples revealed ALTR indicated by immune cell infiltration, accompanied by numerous metal particles (Figure 1C). Spatially resolved multielement mapping by SR-μXRF showed local exposure in all three cases analyzed, characterized by Co- and Cr-containing particles of heterogeneous elemental composition (Figure 1D). The highest Co and Cr signals were detected in peri-implant tissue collected during revision total hip arthroplasty, with minor Co content, i.e., only a few regions indicating colocalized Co and Cr, pointing toward local Co dissolution. XRF spectra of the soft tissue sample, harvested during revision total knee arthroplasty of an exposed versus nonexposed volume indicated arthroprosthetic degradation products characterized by colocalized Co and Cr. The soft tissue sample harvested during revision ankle arthroplasty was characterized by bone residues indicated by high calcium levels. Co-localized Co and Cr were found to be abundant in the soft tissue surrounding osteolytic bone.

Since elemental analyses using SR-μXRF are limited to only a small region of interest, parts of the tissue samples were additionally scanned using SR-μCT to evaluate whether metal debris is distributed throughout the tissue samples. These analyses indicated that exposure to particles of different sizes is evident (Figure 2). Segmentation of micron-sized particles (>116 μm^3) revealed a particle count of 842/250, 1435/250, and 104/250 mm^3 in peri-implant tissue collected during revision surgery of a hip, knee, and ankle arthroplasty implant, respectively.

Taken together, local Co and Cr exposure was evident at the time of revisions of standard hip, knee, and ankle arthroplasty implants, and metal debris is distributed throughout the analyzed peri-implant tissue samples.

To confirm that infiltrating immune cells are macrophages, sections of nine patients (n = 9), including the tree mentioned above, were immunostained (CD45, leukocyte common antigen; CD68, mainly expressed by macrophages; CD14, mainly expressed by monocytic cells) and visualized via confocal laser scanning microscopy (CLSM). Highly autofluorescent metal particles were detected in the tissues of all patients (Figure 3A). Areas with extensive macrophage infiltration were evident in seven out of nine patient tissues analyzed (Figure 3B). All macrophages stained positive for CD14 (Figure 3B). In many cases, macrophages and metal particles colocalized, indicating potential phagocytosis (Figure 3B, lower panel).

3.2. Exposure of Monocytes to Metal Ions Initiates Macrophage Differentiation with a Metal-Specific Imprint. After proving that local exposure to Co and Cr and infiltration of macrophages at the time of aseptic revision of various arthroplasty implants is evident in peri-implant tissue, we next evaluated the effects of Co and Cr ion exposure on human monocytes/macrophages. To this end, primary monocytes were exposed to 1 or 10 $\mu g \times mL^{-1}$ of Co^{2+}, Cr^{3+}, or both metal ions for 48 h, and cell phenotype was analyzed via flow cytometry. In all conditions, monocytes differentiated into macrophages ($CD68^+HLA\text{-}DR^+$; Figure S1). Although the viability of cells dropped following 48 h exposure to high concentrations of Co^{2+}, it did not reach statistical significance compared to nonexposed cells (Figure 4A). Subsequent analyses of surface-expressed CD14, a coreceptor of TLR4, allowed for the discrimination of two subsets: $CD68^+CD14^+$ and $CD68^+CD14^-$ cells (Figure 4B). Exposure of monocytes to 10 $\mu g \times mL^{-1}$ Co^{2+} alone or Co^{2+}/Cr^{3+} combination

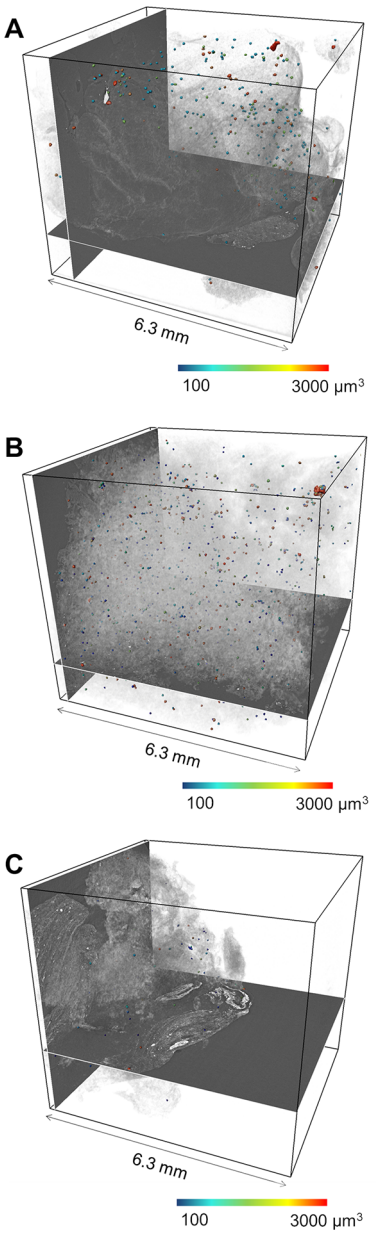

Figure 2. Renderings of SR-μCT data and segmentation of micron-sized debris in peri-implant tissue samples collected during revision surgery of a hip arthroplasty implant (A), knee arthroplasty implant (B), and ankle arthroplasty implant (C). The colors of the debris particles and the color bars indicate the volume of each particle. Please note that for visualization the particles have been dilated using a 3D spherical structuring element of 5 voxels in diameter to enhance the visibility of the particle distribution. The gray transparent cloudlike features are soft-tissue structures.

resulted in a shift from $CD68^+CD14^+$ to mainly $CD68^+CD14^-$ subset (Figure 4B). The subset distribution remained unchanged in all other conditions compared to untreated cells (Figure 4B). Notably, this result was in contrast to the tissue analyses, exclusively showing $CD14^+$ macrophages (Figure 3B). Therefore, the two subsets were further analyzed for the presence of intracellular CD14. Irrespective of the prior analyses dividing macrophages in $CD68^+CD14^+$ and $CD68^+CD14^-$ populations, all cells stained positive for intracellular CD14 (Figures 4C and S2). Therefore, these two subsets are termed $CD68^+CD14^{do+}$ (CD14 double

https://doi.org/10.1021/acsbiomaterials.3c01031
ACS Biomater. Sci. Eng. 2024, 10, 563−574

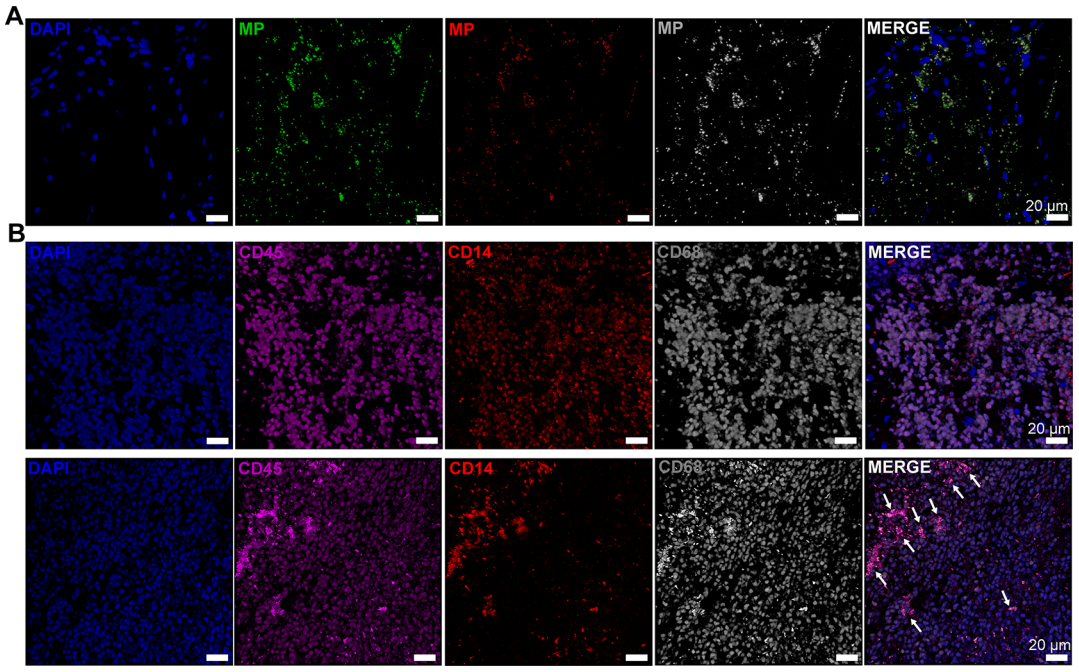

Figure 3. Macrophage infiltration in peri-implant tissue visualized by positive CD45/CD68/CD14 staining and CLSM. (A) Representative reconstruction of CLSM micrographs visualizing highly autofluorescent metal particles (MP) and (B) macrophages (n = 9). Arrows indicate metal particles associated with macrophages.

positive) and $CD68^{+}CD14^{in+}$ (intracellular $CD14^{+}$) in the following. However, both subsets were characterized by reduced expression of intracellular CD14 (Figure S2). Next, the expression of CD16 (FCγRIII) was analyzed. Exposure to high concentrations of Co^{2+} resulted in an almost complete loss of CD16 on the cell surface (Figure 4D).

Next, the stimulatory potential of metal ions toward macrophages was assessed. No activation of macrophages (CD38) in response to any condition was observed (Figure 5A). Irrespective of the macrophage subset, surface expression of HLA-DR was significantly decreased in response to high Co^{2+} concentrations, including coexposure to Co^{2+}/Cr^{3+} (Figure 5B). In contrast, PD-L1 expression remained unaffected under all conditions (Figure 5C).

3.3. Cobalt and Chromium Ions Inhibit Macrophage Response to *Staphylococcus aureus* Infections. Next, the responsiveness of metal-exposed macrophages toward subsequent *S. aureus* infections was assessed. Since *S. aureus* is a common cause of PJIs, MSSA strain 6005 was used. In brief, human primary monocytes were exposed to metal ions for 24 h, subsequently infected with 6005 for 1 h, extracellular bacteria were killed, and macrophage responsiveness was analyzed after 23 additional hours of infection. To match the peri-implant tissue environment, metal exposure continued through the entire series of infections.

First, the phagocytic activity was analyzed by plating intracellular bacteria. Macrophages exposed to 10 $\mu g \times mL^{-1}$ Co^{2+} alone or in combination with Cr^{3+} showed significantly reduced bacterial phagocytosis (Figure 6A). To exclude potential metal ion-mediated bactericidal effects, the 6005 strain was directly exposed to 10 $\mu g \times mL^{-1}$ of metal ions. No effects were observed (Figure S3).

Subsequently, the macrophage phenotype was analyzed in response to infections. Overall, no additional *S. aureus*-mediated cytotoxicity toward macrophages was noted (Figure 6B). Furthermore, the subset distribution ($CD68^{+}CD14^{do+}$ and $CD68^{+}CD14^{in+}$) followed the previously observed metal-mediated phenotype and remained unaffected in all infectious conditions (Figure 6C). Irrespective of infections, general exposure of cells to high concentrations of Co^{2+} resulted in almost a complete loss of CD16 on the cell surface. Of note, infected macrophages exposed to low concentrations of Co^{2+} showed a comparable reduction of CD16 expression (Figure 6D). A similar trend was observed in infections of macrophages with prior Cr^{3+} treatment (Figure 6D).

In addition, the activation of the macrophages was analyzed. While the expansion of $CD38^{+}$ cells was noted in response to infections of naïve cells, all metal ions completely suppressed this activation, irrespective of the type or concentration used (Figure 7A). Overall, no upregulation of HLA-DR expression in response to infection was detected (Figure 7B). In contrast, infection of macrophages led to an upregulation of PD-L1 expression under almost all conditions (Figure 7C). This effect was diminished in infected macrophages that were exposed to 10 $\mu g \times mL^{-1}$ of Co^{2+} alone or in combination with Cr^{3+} (Figure 7C).

Next, the gene expression of different transcription factors and surface markers involved in macrophage activation in response to infection was analyzed. Since mostly single stimulations with high metal ion concentrations, and particularly Co^{2+}, had pronounced effects on macrophage responses, only 10 $\mu g \times mL^{-1}$ of Co^{2+} or Cr^{3+} prior to infection were used. *CD68* mRNA expression, indicative of monocytes to macrophage differentiation, was confirmed in all conditions (Figure S4A). The pro-inflammatory transcriptional factor *STAT1* was upregulated in *S. aureus* infections, while expression of anti-inflammatory *PPARγ* was reduced. In contrast, metal-exposed macrophages expressed similar levels of both transcriptional factors as compared to the unstimulated controls (Figure S4B,C). *IRF5* expression was unaffected under all conditions tested (Figure S4D). In congruence with the flow cytometry analyses, *HLA-DR* mRNA levels were reduced

https://doi.org/10.1021/acsbiomaterials.3c01031
ACS Biomater. Sci. Eng. 2024, 10, 563−574

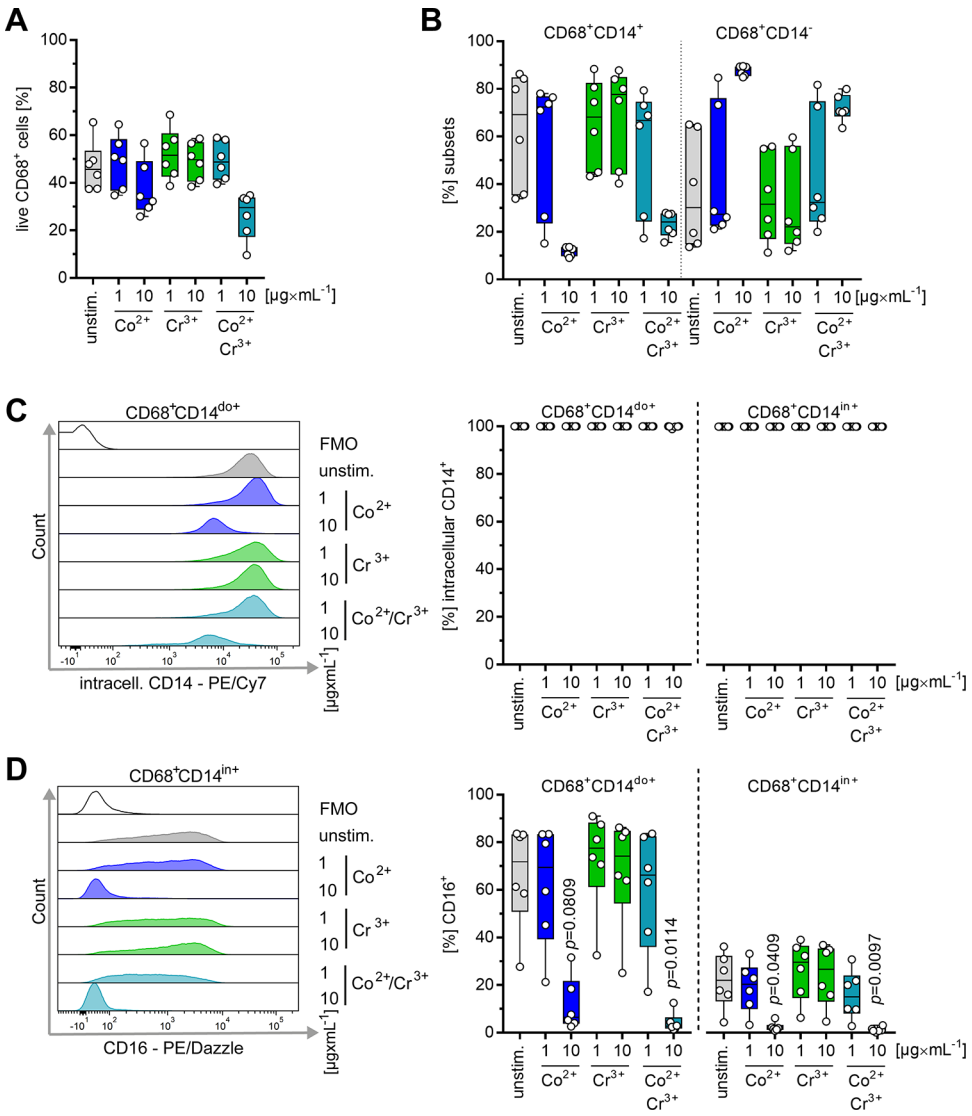

Figure 4. Metal-induced imprinting of macrophage populations. Human primary monocytes were exposed to 1 or 10 $\mu g \times mL^{-1}$ of Co^{2+}, Cr^{3+} alone, or in combination for 48 h. Macrophage viability (A) and subsets (B–D) were analyzed via flow cytometry (n = 6). Representative histograms are shown in (C) and (D) (left panels). (B) Macrophage subsets were evaluated based on intracellular CD68 and extracellular CD14 positivity. (C) Detailed assessment of the subsets was performed based on frequencies of cells, which stained positive for intracellular CD14 ($CD14^+$) and (D) extracellular CD16 ($CD16^+$). The data are displayed as box plots. Each dot represents one independent experiment with cells from one donor. The level of significance was determined using the Kruskal–Wallis test with Dunn's posttest. FMO, fluorescence minus one; unstim., unstimulated control.

particularly in response to Co^{2+} stimulations irrespective of infections (Figure S4E).

4. DISCUSSION

Metal particles and ions derived from orthopedic implants containing CoCrMo can cause ALTRs.[2,50] Tissue necrosis and an influx of lymphocytes and macrophages are regularly observed in neoplastic tissue specimens from patients undergoing aseptic arthroplasty implant revision. Macrophages are crucial first responders to infection and arthroprosthetic particles. They clear pathogens and debris and recruit additional immune cells through the release of chemoattractants. Metal particles and ions were shown to significantly affect macrophage viability.[51] Here, we show that macrophages infiltrate peri-implant tissue of Co/Cr-exposed patients and change their phenotype after Co^{2+} exposure. More strikingly, Co^{2+} affects the expression of various infection-associated surface markers and impairs overall macrophage response to *S. aureus* infection. In contrast, Cr^{3+} does not significantly affect macrophage phenotype but the response to infection. The SR-μXRF and SR-μCT analyses presented here clearly demonstrate that peri-implant tissues, obtained at the time of revision of different implants, are exposed to Co and Cr. In earlier studies, we demonstrated that Co and Cr in peri-implant tissue and fluid obtained during hip arthroplasty implant revisions are present in the particulate and also in the dissociated state,[19,52] with concentrations of up to 25 $\mu g \times mL^{-1}$ of Cr and 7 $\mu g \times mL^{-1}$ of Co in periprosthetic tissue and 9 $\mu g \times mL^{-1}$ of Cr and 15 $\mu g \times mL^{-1}$ of Co in synovial fluid. These data and other studies emphasize not only that the concentrations used for cell stimulations in the present study emulate a clinically relevant exposure scenario but also that Co and Cr released from arthroplasty implants are characterized by a multitude of physicochemical properties,[16−18,21,53] resulting in an interplay

https://doi.org/10.1021/acsbiomaterials.3c01031
ACS Biomater. Sci. Eng. 2024, 10, 563−574

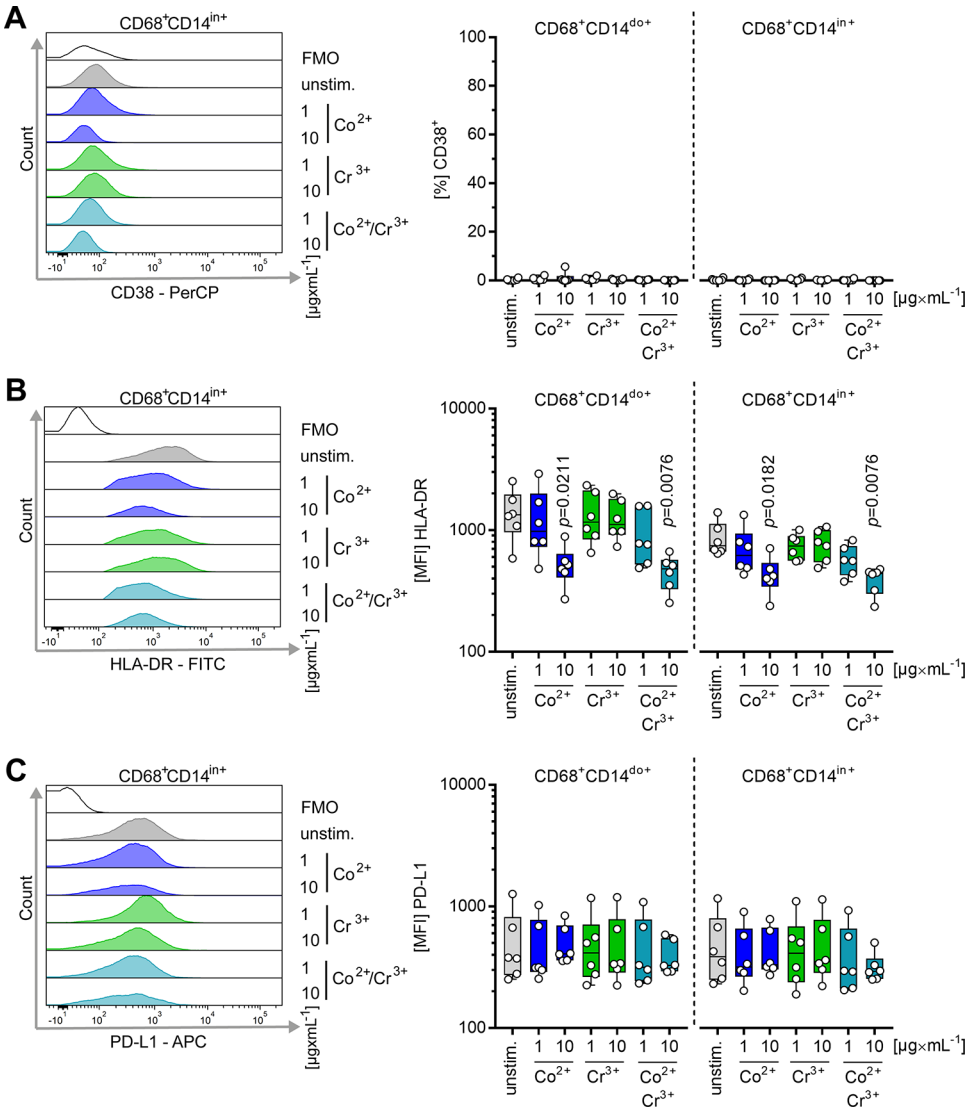

Figure 5. Metal exposure decreases the level of surface expression of HLA-DR on macrophages. Human primary monocytes were exposed to 1 or 10 $\mu g \times mL^{-1}$ of Co^{2+}, Cr^{3+} alone, or in combination for 48 h. Macrophage subsets (A–C) were analyzed via flow cytometry ($n = 6$). Representative histograms are shown in parts (A) and (C) (left panels). The macrophage response to infection and metal exposure was evaluated based on frequencies of $CD38^+$ (A) as well as expression of HLA-DR (B) and PD-L1 (C). The data are displayed as box plots. Each dot represents one independent experiment with cells from one donor. The level of significance was determined using the Kruskal–Wallis test with Dunn's posttest. FMO, fluorescence minus one; unstim., unstimulated control.

of biologically active metal ions and immunogenic particles.[16,54,55] Dense metal aggregation commonly results in tissue inflammation characterized by an influx of macrophages and lymphocytes.[2] Detailed CLSM analyses of patient tissue identified mainly macrophages ($CD45^+CD68^+$ cells), which are often colocalized with metal particles. Subsequently, we determined the phenotype and functionality of macrophages in a series of in vitro experiments using human primary cells. Most studies focus on the cytotoxicity of Co and Cr ions and particles toward different cell types, e.g., fibroblasts, lymphocytes, and different monocytic cell lines.[1] Especially Co was shown to be cytotoxic and necrosis was identified as a predominant type of cell death.[42,56] While Co^{2+} induced cytolytic events in THP1 macrophages, Cr^{3+} did not.[51] This is in line with our results on human primary monocytes/macrophages showing that high concentrations of Co^{2+} are cytotoxic and that Cr^{3+} are not. Characterization of macrophages revealed a substantial shift in subsets from $CD68^+CD14^{do+}$ to $CD68^+CD14^{in+}$ in response to high Co^{2+} concentrations. The latter completely lacked the surface deposition of CD14.

Macrophages phagocytosize metal particles. The acidic pH in the phagolysosome leads to the release of Co^{2+} from Co particles, due to increased solubility of this element at low pH.[57] Consequently, Co^{2+} induces oxidative stress and reactive oxygen species (ROS) production in macrophages.[51,58] Excessive ROS production is in turn linked to impaired macrophage migration.[43] Although speculative, Co^{2+}-mediated stress might impair intracellular protein transport from the ER to the Golgi apparatus, leading to a loss of surface CD14 as well as other markers, including the observed lack of CD16 in our experimental setup, as intracellular stores are not transported to the cell membrane anymore.[59]

Studies have shown that THP1 and U937 monocytic cell lines upregulate transcription of genes encoding for cytokines/chemokines (*IL1B*, *CXCL8*),[51] or release cytokines (IL-6,

https://doi.org/10.1021/acsbiomaterials.3c01031
ACS Biomater. Sci. Eng. 2024, 10, 563–574

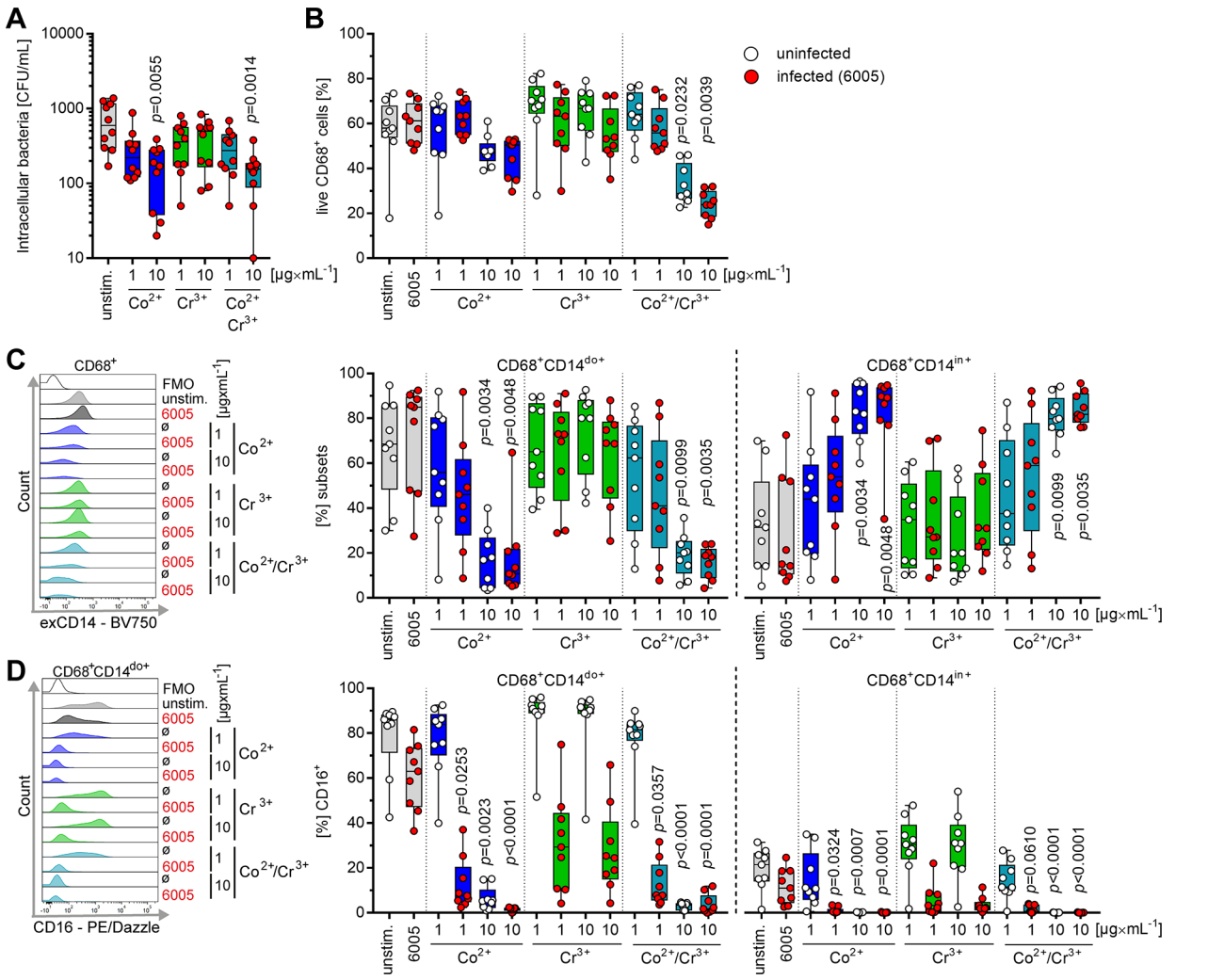

Figure 6. Reduced phagocytosis of bacteria in Co^{2+}-exposed cells. Human macrophages were exposed to 1 or 10 $\mu g \times mL^{-1}$ of Co^{2+} or Cr^{3+} alone or in combination for 24 h. Metal-exposed cells were infected with *S. aureus* 6005 (MOI 1). Extracellular bacteria were killed by substituting the media with antibiotics. Viable intracellular bacteria were determined 2 h post infection (A). Macrophage viability (B) and subsets (C, D) were analyzed via flow cytometry after a total of 48 h of metal treatment with 24 h of infection (n = 10). Representative histograms are shown in left panels of (C) and (D). (C) Analyses of macrophage subsets in response to infections. (D) Frequencies of CD16 positive cells in response to infections. The data are displayed as box plots. Each dot represents one independent experiment with cells from one donor. The level of significance was determined using the Kruskal–Wallis test with Dunn's posttest. FMO, fluorescence minus one; unstim., unstimulated control.

TNFα, IFN-γ)[60] in response to metal exposure. Consequently, this phenomenon has been referred to as "activation". In contrast to those two studies, we did not observe activation of macrophages in response to metal ions since none of the key cellular markers analyzed (CD38, HLA-DR, PD-L1) were upregulated. Even down-regulation of HLA-DR in response to high Co^{2+} concentrations was noted, which was confirmed on the mRNA level. This immunosuppression is further confirmed in infection experiments under constant metal ion exposure. Co^{2+} and Cr^{3+} severely impaired the cellular response to infection. While *S. aureus* infection of naïve cells resulted in the expansion of $CD38^+$ cells, all metal conditions suppressed this effect. In addition, no upregulation of HLA-DR was observed, and PD-L1 upregulation was exclusively impaired when high concentrations of Co^{2+} were used. PD-L1 is a checkpoint inhibitor that binds to PD-1 on T cells. Interaction of these molecules controls T cell activation by preventing excessive proliferation.[40] Our surface markers are further supported by mRNA expression analyses of transcriptional factors. STAT1, a pro-inflammatory transcriptional regulator, expression was exclusively upregulated in *S. aureus* infections without prior metal exposure, while PPARγ, which is rather suppressed under infectious conditions, was down-regulated. In contrast, mRNA expression of these regulators in metal-exposed cells remained at the levels of the unstimulated controls. Therefore, our data support the concept that local exposure to Co^{2+} and Cr^{3+} in human peri-implant tissues suppresses critical immune functions of professional phagocytes and therefore predisposes patients to an increased risk of peri-implant infections, as seen in patients with ALTR.[13,15,25−27] This hypothesis is further supported by our observation that high concentrations of Co^{2+} resulted in a lack of CD16 deposition on the macrophage surface. CD16 is a FcγIII receptor that facilitates phagocytosis of bacteria.[61] Both, lack of surface-associated CD14 as well as CD16 potentially explain the observed reduced bacterial phagocytosis. Of note, *S. aureus* growth itself was not affected by the metal concentrations, suggesting that it might form biofilms in PJIs.[34,35,62−64] PJIs occur in up to 4% of revision arthroplasties.[25] It was reported that the presence of a foreign body and local metal release reduce the infectivity dose of *S.*

https://doi.org/10.1021/acsbiomaterials.3c01031
ACS Biomater. Sci. Eng. 2024, 10, 563−574

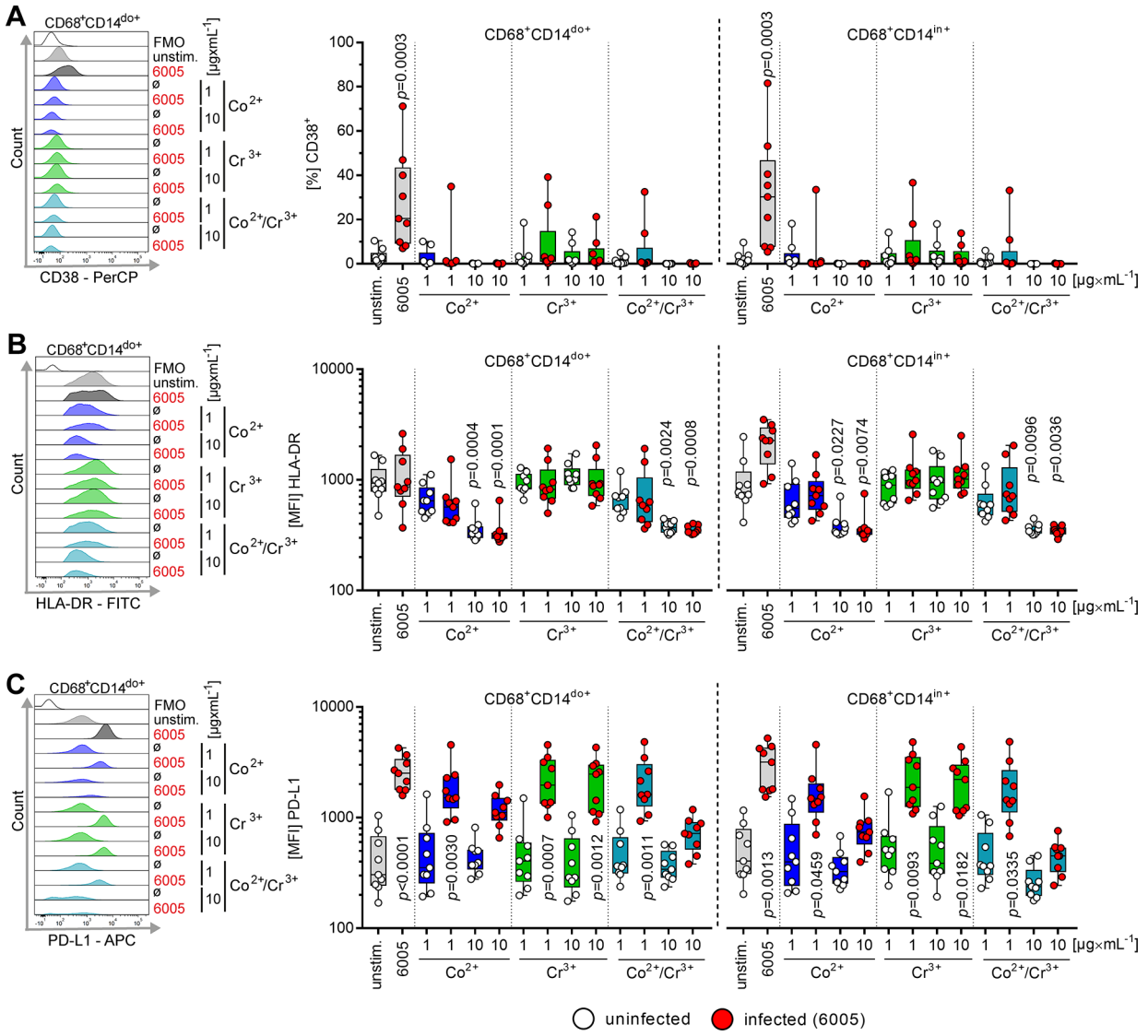

Figure 7. Metal-exposed cells are less responsive to *S. aureus* infections. Human monocytes were exposed to 1 or 10 $\mu g \times mL^{-1}$ of Co^{2+} or Cr^{3+} alone or in combination for 24 h and metal-exposed cells were infected with *S. aureus* 6005 (MOI 1). Macrophage phenotype (A−C) was analyzed via flow cytometry after a total of 48 h of metal treatment, which included 24 h of infection (n = 10). Representative histograms are shown in left panels of panels (A)−(C). The phenotype was evaluated based on frequencies of $CD38^+$ (A) as well as expression of HLA-DR (B) and PD-L1 (C) on the macrophage surface. The data are displayed as box plots. Each dot represents one independent experiment with cells from one donor. The level of significance was determined using the Kruskal−Wallis test with Dunn's posttest. FMO, fluorescence minus one; unstim., unstimulated control.

aureus.[65] Furthermore, a limited number of animal studies revealed reduced phagocytic and bactericidal activities of tissue infiltrating granulocytes induced by nonphagocytosable foreign bodies, while circulating neutrophils retained the activities.[66,67] Our in vitro data support these findings and underline the need for additional investigations analyzing ex vivo metal-mediated local immunosuppressive effects and their consequences for potential local infections. In addition, further prospective clinical studies are warranted.

5. CONCLUSIONS

In conclusion, our results provide evidence that exposure to Co and Cr ions inhibits essential immune functions of professional phagocytes. This finding potentially explains the increased risk of PJIs following revision arthroplasty. CoCrMo is a metallic biomaterial that is constantly used in orthopedic surgery. Degradation of this applied metallic biomaterial leading to systemic and local metal exposure and ALTR is a clinically well-known scenario. Based on our data, a risk assessment for PJI, especially for infections with *S. aureus*, after the use of CoCrMo-containing arthroplasty implants in prospectively designed studies seems indicated. In addition, in vitro studies on Co and Cr in the particulate state and ex vivo studies on the classical pro- and anti-inflammatory phenotype as well as the functionality of macrophages locally exposed to metal ions and particles should be performed. Our data support a better understanding of the local tissue response after material degradation and add weight to the risk and benefit evaluation of CoCrMo routinely used in arthroplasty. Possible long-term effects of metal-based biomaterial degradation including the risk of infection should be considered.

https://doi.org/10.1021/acsbiomaterials.3c01031
ACS Biomater. Sci. Eng. 2024, 10, 563−574

■ ASSOCIATED CONTENT

Supporting Information

The Supporting Information is available free of charge at https://pubs.acs.org/doi/10.1021/acsbiomaterials.3c01031.

Extended results: gating strategy used to identify human monocytes/macrophages; intracellular CD14 expression in macrophages; impact of metal ions on *Staphylococcus aureus* vitality; and gene expression analyses in macrophages (PDF)

■ AUTHOR INFORMATION

Corresponding Authors

Nikolai Siemens − *Department of Molecular Genetics and Infection Biology, University of Greifswald, Greifswald 17489, Germany;* orcid.org/0000-0003-0657-3822; Email: nikolai.siemens@uni-greifswald.de

Janosch Schoon − *Center for Orthopaedics, Trauma Surgery and Rehabilitation Medicine, University Medicine Greifswald, Greifswald 17475, Germany;* orcid.org/0000-0003-2337-0795; Email: janosch.schoon@med.uni-greifswald.de

Authors

Lea A. Tölken − *Department of Molecular Genetics and Infection Biology, University of Greifswald, Greifswald 17489, Germany*

Georgi I. Wassilew − *Center for Orthopaedics, Trauma Surgery and Rehabilitation Medicine, University Medicine Greifswald, Greifswald 17475, Germany*

Daniel Grolimund − *Swiss Light Source, Paul Scherrer Institute, Villigen-PSI 5232, Switzerland;* orcid.org/0000-0001-9721-7940

Timm Weitkamp − *Synchrotron SOLEIL, Saint-Aubin 91190, France*

Bernhard Hesse − *Xploraytion GmbH, Berlin 10625, Germany; ESRF-The European Synchrotron, Grenoble 38000, France*

Anastasia Rakow − *Center for Orthopaedics, Trauma Surgery and Rehabilitation Medicine, University Medicine Greifswald, Greifswald 17475, Germany;* orcid.org/0000-0001-6171-8292

Complete contact information is available at: https://pubs.acs.org/10.1021/acsbiomaterials.3c01031

Author Contributions

[▽]N.S. and J.S. equally contributed to this work.

Author Contributions

Conceptualization: L.A.T., N.S., J.S.; data curation: L.A.T., N.S., J.S.; formal analysis: L.A.T., N.S., J.S.; funding acquisition: N.S., G.I.W., J.S.; investigation: L.A.T., N.S., J.S., B.H., T.W., A.R., D.G.; methodology: N.S., J.S., B.H., T.W., D.G.; project administration: N.S., J.S.; resources: G.I.W., N.S., J.S.; software: G.I.W., N.S., J.S.; supervision: N.S., J.S.; validation: L.A.T., G.I.W., A.R., N.S.; J.S.; visualization: L.A.T., N.S., J.S.; writing—original draft: L.A.T., N.S., J.S.; writing—review and editing: L.A.T., G.I.W., A.R., N.S., J.S., T.W., B.H., D.G.

Funding

This work was supported by German Research Foundation (DFG; grants 407176682 to N.S., 492903360 to N.S., and INST 292/151-1 FUGG - 447143887 for the purchase of CLSM). J.S. received the Domagk Master Class (DMC) scholarship funded by the University Medicine Greifswald.

Notes

The authors declare the following competing financial interest(s): GIW serves as consultant for Mathys AG and receives institutional funding and research support from Mathys AG and Smith & Nephew. These companies did not financially support this study, had no role in study design, sample collection, data collection and analysis, decision to publish, or preparation of the manuscript. All other authors declare no competing interest.

■ ACKNOWLEDGMENTS

This study was supported with beamtime at Synchrotron SOLEIL (ANATOMIX, proposal number: 20220776) and Swiss Light Source (microXAS, proposal number: 20201651). ANATOMIX is an Equipment of Excellence (EQUIPEX) funded by the *Investments for the Future* program of the French National Research Agency (ANR), project *NanoimagesX*, grant no. ANR-11-EQPX-0031. The authors would like to thank D. Stobbe, L. Berndt, and K. Barnekow for expert technical support. The authors gratefully acknowledge support during SR-μCT data analyses by Dr. E. Bortel and acquisition by Dr. C. Seim, Dr. E. Bortel, and Javier Gerber as well as during SR-XRF data acquisition by Dr. F. Ferreira Sanchez, Dr. C. Seim, and L. Schweitzer. Furthermore, the authors would like to thank PD Dr. Dr. J. Reichert, Dr. A. Hofer, Dr. U. Schietsch, and Dr. A. Springer for intraoperative sample harvesting. All patients are gratefully acknowledged for their participation in the study.

■ ABBREVIATIONS

ALTR, adverse local tissue reaction; CLSM, confocal laser scanning microscopy; CoCrMo, cobalt−chromium−molybdenum; FMO, fluorescence minus one; PBS, phosphate-buffered saline; PJI, periprosthetic joint infection; SR-μCT, synchrotron radiation microcomputed tomography; SR-μXRF, synchrotron radiation micro X-ray fluorescence analyses

■ REFERENCES

(1) Liu, Z.; Liu, H.; Vowden, R.; Hughes, L.; Qi, D.; Francis, W.; Perino, G.; Pink, R.; Xiao, J.; Li, B.; Xia, Z. Combination of cobalt, chromium and titanium nanoparticles increases cytotoxicity in vitro and pro-inflammatory cytokines in vivo. *Journal of Orthopaedic Translation* **2023**, *38*, 203−212.

(2) Perino, G.; De Martino, I.; Zhang, L.; Xia, Z.; Gallo, J.; Natu, S.; Langton, D.; Huber, M.; Rakow, A.; Schoon, J.; Gomez-Barrena, E.; Krenn, V. The contribution of the histopathological examination to the diagnosis of adverse local tissue reactions in arthroplasty. *EFORT Open Rev.* **2021**, *6* (6), 399−419.

(3) Catelas, I.; Petit, A.; Vali, H.; Fragiskatos, C.; Meilleur, R.; Zukor, D. J.; Antoniou, J.; Huk, O. L. Quantitative analysis of macrophage apoptosis vs. necrosis induced by cobalt and chromium ions in vitro. *Biomaterials* **2005**, *26* (15), 2441−2453.

(4) Eltit, F.; Wang, Q.; Wang, R. Mechanisms of adverse local tissue reactions to hip implants. *Front. Bioeng. Biotechnol.* **2019**, *7*, 176.

(5) Nyga, A.; Hart, A.; Tetley, T. D. Importance of the HIF pathway in cobalt nanoparticle-induced cytotoxicity and inflammation in human macrophages. *Nanotoxicology* **2015**, *9* (7), 905−917.

(6) Jämsen, E.; Pajarinen, J.; Kouri, V.-P.; Rahikkala, A.; Goodman, S. B.; Manninen, M.; Nordström, D. C.; Eklund, K. K.; Nurmi, K. Tumor necrosis factor primes and metal particles activate the NLRP3 inflammasome in human primary macrophages. *Acta biomaterialia* **2020**, *108*, 347−357.

(7) Couto, M.; Vasconcelos, D. P.; Sousa, D. M.; Sousa, B.; Conceição, F.; Neto, E.; Lamghari, M.; Alves, C. J. The mechanisms underlying the biological response to wear debris in periprosthetic inflammation. *Front. Mater.* **2020**, *7*, 274.
(8) Bonner, B.; Arauz, P.; Klemt, C.; Kwon, Y.-M. Outcome of re-revision surgery for adverse local tissue reaction in metal-on-polyethylene and metal-on-metal total hip arthroplasty. *Journal of arthroplasty* **2020**, *35* (6), S284−S288.
(9) Munro, J. T.; Masri, B. A.; Duncan, C. P.; Garbuz, D. S. High Complication Rate After Revision of Large-head Metal-on-metal Total Hip Arthroplasty. *Clin. Orthop. Relat. Res.* **2014**, *472* (2), 523−528.
(10) Matharu, G. S.; Pynsent, P. B.; Sumathi, V. P.; Mittal, S.; Buckley, C. D.; Dunlop, D. J.; Revell, P. A.; Revell, M. P. Predictors of time to revision and clinical outcomes following revision of metal-on-metal hip replacements for adverse reaction to metal debris. *Bone & Joint Journal* **2014**, *96-B* (12), 1600−1609.
(11) Matharu, G. S.; Judge, A.; Murray, D. W.; Pandit, H. G. Outcomes After Metal-on-metal Hip Revision Surgery Depend on the Reason for Failure: A Propensity Score-matched Study. *Clin. Orthop. Relat. Res.* **2018**, *476* (2), 245−258.
(12) Grammatopolous, G.; Pandit, H.; Kwon, Y. M.; Gundle, R.; McLardy-Smith, P.; Beard, D. J.; Murray, D. W.; Gill, H. S. Hip resurfacings revised for inflammatory pseudotumour have a poor outcome. *Journal of Bone & Joint Surgery British Volume* **2009**, *91-B* (8), 1019−1024.
(13) Wyles, C. C.; Van Demark, R. E.; Sierra, R. J.; Trousdale, R. T. High Rate of Infection After Aseptic Revision of Failed Metal-on-Metal Total Hip Arthroplasty. *Clin. Orthop. Relat. Res.* **2014**, *472* (2), 509−516.
(14) Chang, J. S.; Haddad, F. S. Revision total hip arthroplasty for metal-on-metal failure. *Journal of Clinical Orthopaedics and Trauma* **2020**, *11* (1), 9−15.
(15) Matharu, G. S.; Judge, A.; Murray, D. W.; Pandit, H. G. Outcomes following revision surgery performed for adverse reactions to metal debris in non-metal-on-metal hip arthroplasty patients. *Bone & Joint Research* **2017**, *6* (7), 405−413.
(16) Schulze, F.; Perino, G.; Rakow, A.; Wassilew, G.; Schoon, J. Noninfectious tissue interactions at periprosthetic interfaces. *Orthopädie* **2023**, *52*, 186.
(17) Schoon, J.; Hesse, B.; Rakow, A.; Ort, M. J.; Lagrange, A.; Jacobi, D.; Winter, A.; Huesker, K.; Reinke, S.; Cotte, M.; Tucoulou, R.; Marx, U.; Perka, C.; Duda, G. N.; Geissler, S. Metal-Specific Biomaterial Accumulation in Human Peri-Implant Bone and Bone Marrow. *Adv. Sci.* **2020**, *7* (20), No. 2000412.
(18) Morrell, A. P.; Floyd, H.; JF, W. M.; Grover, L. M.; Castillo-Michel, H.; Davis, E. T.; Parker, J. E.; Martin, R. A.; Addison, O. Improving our understanding of metal implant failures: Multiscale chemical imaging of exogenous metals in ex-vivo biological tissues. *Acta Biomater.* **2019**, *98*, 284−293.
(19) Rakow, A.; Schoon, J.; Dienelt, A.; John, T.; Textor, M.; Duda, G.; Perka, C.; Schulze, F.; Ode, A. Influence of particulate and dissociated metal-on-metal hip endoprosthesis wear on mesenchymal stromal cells in vivo and in vitro. *Biomaterials* **2016**, *98*, 31−40.
(20) Espallargas, N.; Torres, C.; Muñoz, A. I. A metal ion release study of CoCrMo exposed to corrosion and tribocorrosion conditions in simulated body fluids. *Wear* **2015**, *332*, 669−678.
(21) Schoon, J.; Hesse, B.; Tucoulou, R.; Geissler, S.; Ort, M.; Duda, G. N.; Perka, C.; Wassilew, G. I.; Perino, G.; Rakow, A. Synchrotron-based characterization of arthroprosthetic CoCrMo particles in human bone marrow. *J. Mater. Sci. Mater. Med.* **2022**, *33* (6), 54.
(22) Gkiatas, I.; Sharma, A. K.; Greenberg, A.; Duncan, S. T.; Chalmers, B. P.; Sculco, P. K. Serum metal ion levels in modular dual mobility acetabular components: a systematic review. *Journal of Orthopaedics* **2020**, *21*, 432−437.
(23) Rakow, A.; Schoon, J. Systemic effects of metals released from arthroplasty implants−a brief summary. *Zeitschrift für Orthopädie und Unfallchirurgie* **2020**, *158* (05), 501−507.
(24) Bradberry, S.; Wilkinson, J.; Ferner, R. Systemic toxicity related to metal hip prostheses. *Clinical toxicology* **2014**, *52* (8), 837−847.
(25) Izakovicova, P.; Borens, O.; Trampuz, A. Periprosthetic joint infection: current concepts and outlook. *EFORT Open Rev.* **2019**, *4* (7), 482−494.
(26) Kong, L.; Cao, J.; Zhang, Y.; Ding, W.; Shen, Y. Risk factors for periprosthetic joint infection following primary total hip or knee arthroplasty: a meta-analysis. *Int. Wound J.* **2017**, *14* (3), 529−536.
(27) McMaster Arthroplasty, C. Risk Factors for Periprosthetic Joint Infection Following Primary Total Hip Arthroplasty: A 15-Year, Population-Based Cohort Study. *J. Bone Jt. Surg.* **2020**, *102* (6), 503−509.
(28) Renz, N.; Trampuz, A.; Perka, C.; Rakow, A. In *Outcome and Failure Analysis of 132 Episodes of Hematogenous Periprosthetic Joint Infections—A Cohort Study, Open Forum Infectious Diseases*; Oxford University Press US, 2022; p ofac094.
(29) Dale, H.; Hovding, P.; Tveit, S. M.; Graff, J. B.; Lutro, O.; Schrama, J. C.; Wik, T. S.; Skramm, I.; Westberg, M.; Fenstad, A. M.; Hallan, G.; Engesaeter, L. B.; Furnes, O. Increasing but levelling out risk of revision due to infection after total hip arthroplasty: a study on 108,854 primary THAs in the Norwegian Arthroplasty Register from 2005 to 2019. *Acta Orthop* **2021**, *92* (2), 208−214.
(30) Kurtz, S. M.; Lau, E. C.; Son, M. S.; Chang, E. T.; Zimmerli, W.; Parvizi, J. Are We Winning or Losing the Battle With Periprosthetic Joint Infection: Trends in Periprosthetic Joint Infection and Mortality Risk for the Medicare Population. *J. Arthroplasty* **2018**, *33* (10), 3238−3245.
(31) Saavedra-Lozano, J.; Falup-Pecurariu, O.; Faust, S. N.; Girschick, H.; Hartwig, N.; Kaplan, S.; Lorrot, M.; Mantadakis, E.; Peltola, H.; Rojo, P.; Zaoutis, T.; LeMair, A. Bone and Joint Infections. *Pediatric Infectious Disease Journal* **2017**, *36* (8), 788−799.
(32) Tong, S. Y.; Davis, J. S.; Eichenberger, E.; Holland, T. L.; Fowler, V. G., Jr Staphylococcus aureus infections: epidemiology, pathophysiology, clinical manifestations, and management. *Clin. Microbiol. Rev.* **2015**, *28* (3), 603−661.
(33) Liukkonen, R.; Honkanen, M.; Reito, A.; Skyttä, E.; Karppelin, M.; Eskelinen, A. Trends in Revision Hip Arthroplasty for Prosthetic Joint Infection: A Single-Center Study of 423 Hips at a High-Volume Center between 2008 and 2021. *J. Arthroplasty* **2023**, *38*, 1151 DOI: 10.1016/j.arth.2023.02.061.
(34) Patel, R. Periprosthetic Joint Infection. *New England Journal of Medicine* **2023**, *388* (3), 251−262.
(35) Tande, A. J.; Patel, R. Prosthetic Joint Infection. *Clin. Microbiol. Rev.* **2014**, *27* (2), 302−345.
(36) Reipi Group for the Study of Prosthetic Joint Infections/Benito, N.; Mur, I.; Ribera, A.; Soriano, A.; Rodriguez-Pardo, D.; Sorli, L.; Cobo, J.; Fernandez-Sampedro, M.; Del Toro, M. D.; Guio, L.; Praena, J.; Bahamonde, A.; Riera, M.; Esteban, J.; Baraia-Etxaburu, J. M.; Martinez-Alvarez, J.; Jover-Saenz, A.; Duenas, C.; Ramos, A.; Sobrino, B.; Euba, G.; Morata, L.; Pigrau, C.; Horcajada, J. P.; Coll, P.; Crusi, X.; Ariza, J.; Geio, S. The Different Microbial Etiology of Prosthetic Joint Infections according to Route of Acquisition and Time after Prosthesis Implantation, Including the Role of Multidrug-Resistant Organisms. *J. Clin. Med.* **2019**, *8* (5), 673.
(37) Tai, D. B. G.; Patel, R.; Abdel, M. P.; Berbari, E. F.; Tande, A. J. Microbiology of hip and knee periprosthetic joint infections: a database study. *Clin Microbiol Infect* **2022**, *28* (2), 255−259.
(38) Triffault-Fillit, C.; Ferry, T.; Laurent, F.; Pradat, P.; Dupieux, C.; Conrad, A.; Becker, A.; Lustig, S.; Fessy, M. H.; Chidiac, C.; Valour, F.; Lyon, B. J. I. S. G. Microbiologic epidemiology depending on time to occurrence of prosthetic joint infection: a prospective cohort study. *Clin. Microbiol. Infect.* **2019**, *25* (3), 353−358.
(39) Nich, C.; Takakubo, Y.; Pajarinen, J.; Ainola, M.; Salem, A.; Sillat, T.; Rao, A. J.; Raska, M.; Tamaki, Y.; Takagi, M.; Konttinen, Y. T.; Goodman, S. B.; Gallo, J. Macrophages—Key cells in the response to wear debris from joint replacements. *J. Biomed. Mater. Res., Part A* **2013**, *101* (10), 3033−3045.

(40) Locati, M.; Curtale, G.; Mantovani, A. Diversity, Mechanisms, and Significance of Macrophage Plasticity. *Annual Review of Pathology: Mechanisms of Disease* **2020**, *15* (1), 123−147.
(41) Gentek, R.; Molawi, K.; Sieweke, M. H. Tissue macrophage identity and self-renewal. *Immunological Reviews* **2014**, *262* (1), 56−73.
(42) Horev-Azaria, L.; Kirkpatrick, C. J.; Korenstein, R.; Marche, P. N.; Maimon, O.; Ponti, J.; Romano, R.; Rossi, F.; Golla-Schindler, U.; Sommer, D.; Uboldi, C.; Unger, R. E.; Villiers, C. Predictive Toxicology of Cobalt Nanoparticles and Ions: Comparative In Vitro Study of Different Cellular Models Using Methods of Knowledge Discovery from Data. *Toxicol. Sci.* **2011**, *122* (2), 489−501.
(43) Xu, J.; Yang, J.; Nyga, A.; Ehteramyan, M.; Moraga, A.; Wu, Y.; Zeng, L.; Knight, M. M.; Shelton, J. C. Cobalt (II) ions and nanoparticles induce macrophage retention by ROS-mediated down-regulation of RhoA expression. *Acta biomaterialia* **2018**, *72*, 434−446.
(44) Weitkamp, T.; Scheel, M.; Perrin, J.; Daniel, G.; King, A.; Le Roux, V.; Giorgetta, J.; Carcy, A.; Langlois, F.; Desjardins, K. Microtomography on the ANATOMIX beamline at Synchrotron SOLEIL. *J. Phys.: Conf. Ser.* **2022**, *2380*, No. 012122, DOI: 10.1088/1742-6596/2380/1/012122.
(45) Weitkamp, T.; Scheel, M.; Giorgetta, J.; Joyet, V.; Le Roux, V.; Cauchon, G.; Moreno, T.; Polack, F.; Thompson, A.; Samama, J. The tomography beamline ANATOMIX at Synchrotron SOLEIL. *J. Phys.: Conf. Ser.* **2017**, *849*, No. 012037, DOI: 10.1088/1742-6596/849/1/012037.
(46) Solé, V. A.; Papillon, E.; Cotte, M.; Walter, P.; Susini, J. A multiplatform code for the analysis of energy-dispersive X-ray fluorescence spectra. *Spectrochimica Acta Part B: Atomic Spectroscopy* **2007**, *62* (1), 63−68.
(47) Wick, M. R. *In The hematoxylin and eosin stain in anatomic pathology—An often-neglected focus of quality assurance in the laboratory, Seminars in diagnostic pathology*; Elsevier, 2019; pp 303−311.
(48) Group, I. S. Baude, J.; Bastien, S.; Gillet, Y.; Leblanc, P.; Itzek, A.; Tristan, A.; Bes, M.; Duguez, S.; Moreau, K.; Diep, B. A.; Norrby-Teglund, A.; Henry, T.; Vandenesch, F. Necrotizing Soft Tissue Infection Staphylococcus aureus but not S. pyogenes Isolates Display High Rates of Internalization and Cytotoxicity Toward Human Myoblasts. *J. Infect. Dis.* **2019**, *220* (4), 710−719.
(49) Mairpady Shambat, S.; Siemens, N.; Monk, I. R.; Mohan, D. B.; Mukundan, S.; Krishnan, K. C.; Prabhakara, S.; Snall, J.; Kearns, A.; Vandenesch, F.; Svensson, M.; Kotb, M.; Gopal, B.; Arakere, G.; Norrby-Teglund, A. A point mutation in AgrC determines cytotoxic or colonizing properties associated with phenotypic variants of ST22 MRSA strains. *Sci. Rep.* **2016**, *6*, 31360.
(50) Krenn, V.; Perino, G. Histological Diagnosis of Implant-Associated Pathologies. In *Histological Diagnosis of Implant-Associated Pathologies*, Krenn, V.; Perino, G., Eds.; Springer: Berlin Heidelberg: Berlin, Heidelberg, 2017; pp 1−44.
(51) Loeffler, H.; Jonitz-Heincke, A.; Peters, K.; Mueller-Hilke, B.; Fiedler, T.; Bader, R.; Klinder, A. Comparison of Inflammatory Effects in THP-1 Monocytes and Macrophages after Exposure to Metal Ions. *Materials* **2020**, *13* (5), 1150.
(52) Schoon, J.; Geißler, S.; Traeger, J.; Luch, A.; Tentschert, J.; Perino, G.; Schulze, F.; Duda, G. N.; Perka, C.; Rakow, A. Multi-elemental nanoparticle exposure after tantalum component failure in hip arthroplasty: in-depth analysis of a single case. *Nanomedicine: Nanotechnology, Biology and Medicine* **2017**, *13* (8), 2415−2423.
(53) Xia, Z.; Ricciardi, B. F.; Liu, Z.; von Ruhland, C.; Ward, M.; Lord, A.; Hughes, L.; Goldring, S. R.; Purdue, E.; Murray, D. Nano-analyses of wear particles from metal-on-metal and non-metal-on-metal dual modular neck hip arthroplasty. *Nanomedicine* **2017**, *13* (3), 1205−1217.
(54) Perino, G.; Sunitsch, S.; Huber, M.; Ramirez, D.; Gallo, J.; Vaculova, J.; Natu, S.; Kretzer, J.; Müller, S.; Thomas, P. Diagnostic guidelines for the histological particle algorithm in the periprosthetic neo-synovial tissue. *BMC Clin. Pathol.* **2018**, *18* (1), 7.
(55) Pearson, M. J.; Williams, R. L.; Floyd, H.; Bodansky, D.; Grover, L. M.; Davis, E. T.; Lord, J. M. The effects of cobalt−chromium−molybdenum wear debris in vitro on serum cytokine profiles and T cell repertoire. *Biomaterials* **2015**, *67*, 232−239.
(56) Granchi, D.; Cenni, E.; Ciapetti, G.; Savarino, L.; Stea, S.; Gamberini, S.; Gori, A.; Pizzoferrato, A. Cell death induced by metal ions: necrosis or apoptosis? *J. Mater. Sci.: Mater. Med.* **1998**, *9*, 31−37.
(57) Posada, O. M.; Tate, R. J.; Meek, R. M. D.; Grant, M. H. In Vitro Analyses of the Toxicity, Immunological, and Gene Expression Effects of Cobalt-Chromium Alloy Wear Debris and Co Ions Derived from Metal-on-Metal Hip Implants. *Lubricants [Online]* **2015**, *3*, 539−568.
(58) Scharf, B.; Clement, C. C.; Zolla, V.; Perino, G.; Yan, B.; Elci, S. G.; Purdue, E.; Goldring, S.; Macaluso, F.; Cobelli, N.; Vachet, R. W.; Santambrogio, L. Molecular analysis of chromium and cobalt-related toxicity. *Sci. Rep.* **2014**, *4* (1), 5729.
(59) Yoshioka, N.; Taniguchi, Y.; Yoshida, A. Y. A.; Nakata, K.; Nishizawa, T.; Inagawa, H.; Kohchi, C.; Soma, G.-I. Intracellular Localization of CD14 Protein in Intestinal Macrophages. *Anticancer Res.* **2009**, *29* (3), 865.
(60) Posada, O. M.; Tate, R. J.; Grant, M. H. Effects of CoCr metal wear debris generated from metal-on-metal hip implants and Co ions on human monocyte-like U937 cells. *Toxicology in Vitro* **2015**, *29* (2), 271−280.
(61) Nagarajan, S.; Chesla, S.; Cobern, L.; Anderson, P.; Zhu, C.; Selvaraj, P. Ligand Binding and Phagocytosis by CD16 (Fc γ Receptor III) Isoforms: PHAGOCYTIC SIGNALING BY ASSOCIATED ζ AND γ SUBUNITS IN CHINESE HAMSTER OVARY CELLS (∗). *J. Biol. Chem.* **1995**, *270* (43), 25762−25770.
(62) Frank Kristi, L.; Hanssen Arlen, D.; Patel, R. icaA Is Not a Useful Diagnostic Marker for Prosthetic Joint Infection. *J. Clin. Microbiol.* **2004**, *42* (10), 4846−4849.
(63) Lu, Y.; Cai, W.-J.; Ren, Z.; Han, P. The Role of Staphylococcal Biofilm on the Surface of Implants in Orthopedic Infection Microorganisms [Online], 2022.
(64) Yamada, K. J.; Heim, C. E.; Xi, X.; Attri, K. S.; Wang, D.; Zhang, W.; Singh, P. K.; Bronich, T. K.; Kielian, T. Monocyte metabolic reprogramming promotes pro-inflammatory activity and Staphylococcus aureus biofilm clearance. *PLOS Pathogens* **2020**, *16* (3), No. e1008354.
(65) Gbejuade, H. O.; Lovering, A. M.; Webb, J. C. The role of microbial biofilms in prosthetic joint infections. *Acta Orthop* **2015**, *86* (2), 147−58.
(66) Zimmerli, W.; Lew, P. D.; Waldvogel, F. A. Pathogenesis of foreign body infection. Evidence for a local granulocyte defect. *J. Clin Invest* **1984**, *73* (4), 1191−200.
(67) Zimmerli, W.; Waldvogel, F. A.; Vaudaux, P.; Nydegger, U. E. Pathogenesis of foreign body infection: description and characteristics of an animal model. *J. Infect Dis* **1982**, *146* (4), 487−97.

Supporting Information

Cobalt and chromium ions impair macrophage response to *Staphylococcus aureus* infection

Lea A. Tölken[a], Georgi I. Wassilew[b], Daniel Grolimund[c], Timm Weitkamp[d], Bernhard Hesse[e,f], Anastasia Rakow[b], Nikolai Siemens[a, ‡], and Janosch Schoon[b, ‡]**

[a] Department of Molecular Genetics and Infection Biology, University of Greifswald, 17489 Greifswald, Germany.

[b] Center for Orthopaedics, Trauma Surgery and Rehabilitation Medicine, University Medicine Greifswald, 17475 Greifswald, Germany

[c] Swiss Light Source, Paul Scherrer Institute, 5232 Villigen-PSI, Switzerland

[d] Synchrotron SOLEIL, 91190 Saint-Aubin, France

[e] Xploraytion GmbH, 10625 Berlin, Germany

[f] ESRF-The European Synchrotron, 38000, Grenoble, France

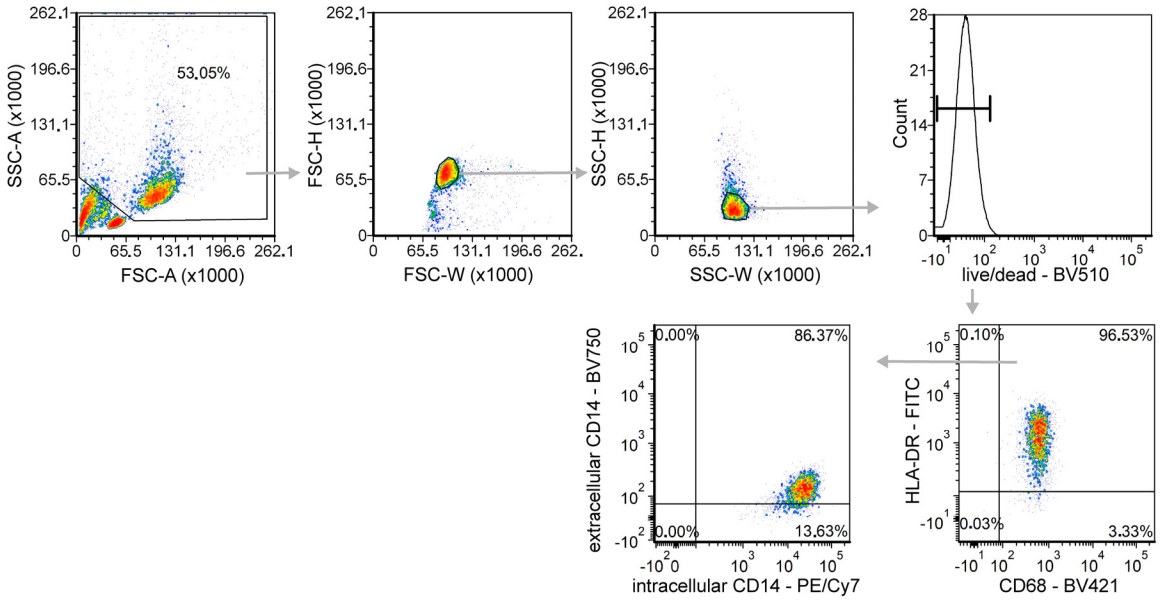

Figure S1. Gating strategy used to identify human monocytes/macrophages. Doublets were excluded by consecutive gating of FSC-H/FSC-W and SSC-H/SSC-W. Dead cells were excluded by using the Zombie Aqua™ Fixable Viability Kit. Monocytes/macrophages were selected based on the expression of HLA-DR and CD68. Macrophage subsets were further distinguished based on expression of intracellular and extracellular CD14.

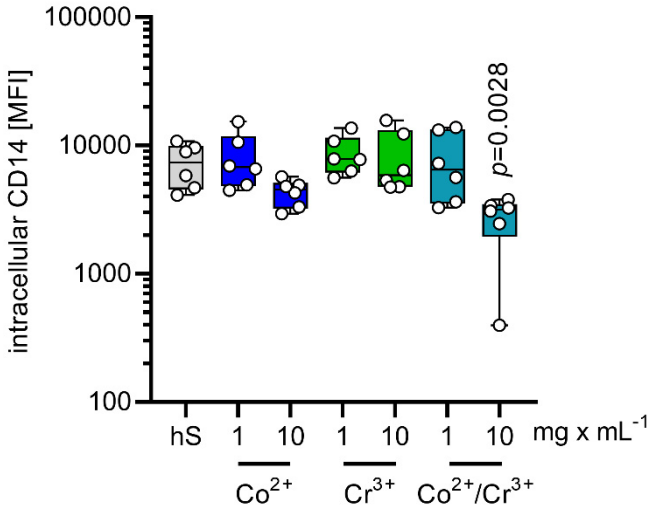

Figure S2. Intracellular CD14 expression in macrophages. Human primary monocytes were exposed to 1 or 10 µg×mL^{-1} of Co^{2+}, Cr^{3+} alone or in combination for 48 h and expression of intracellular CD14 was analyzed via flow cytometry (n=6). The data are displayed as box plots. Each dot represents one independent experiment with cells from one donor. The level of significance was determined using Kruskal-Wallis test with Dunn's posttest. FMO, fluorescence minus one; unstim., unstimulated control.

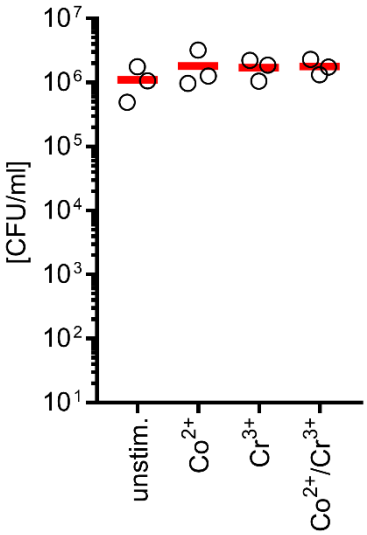

Figure S3. The impact of 10 µg×mL^{-1} of indicated metal ions on *Staphylococcus aureus* vitality. In short, 1x10^6 bacteria were incubated with 10 µg×mL^{-1} of indicated metal ions for 1 h at 37°C. Viable bacteria were plated on blood agar plates (n=3). unstim., unstimulated control.

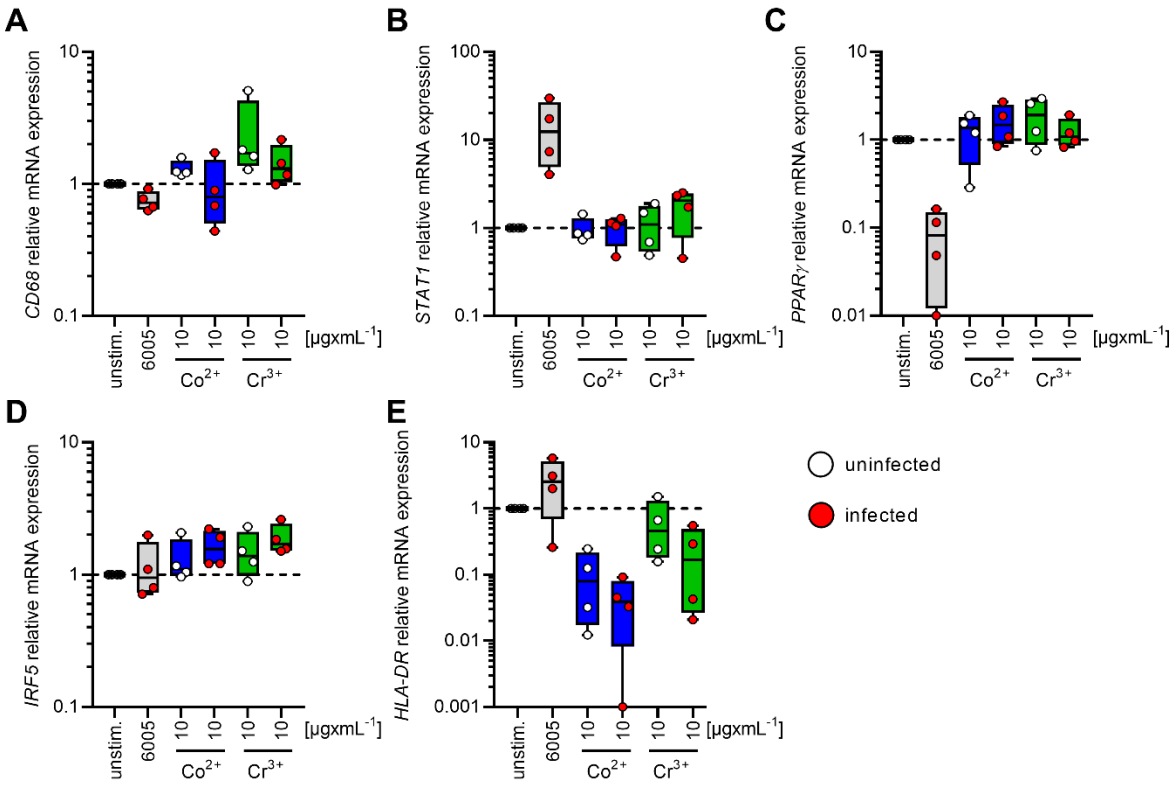

Figure S4. Gene expression analyses in macrophages. Human primary monocytes were exposed to 10 µg×mL^{-1} of Co^{2+} or Cr^{3+} for 48 h. Metal-exposed cells were infected with *S. aureus* 6005 (MOI 1). Extracellular bacteria were killed by substituting the media with antibiotics. Gene expression of genes encoding for *CD68* (A), *STAT1* (B), *PPARγ* (C), *IRF5* (D), and *HLA-DR* (E) are shown. The data are displayed as box plots. Each dot represents one independent experiment with cells from one donor (n=4). unstim., unstimulated control.